HEAT TRANSFER BY IMPINGEMENT COOLING OF SPUR GEARS

Christian Kromer, Felix von Plehwe, Laura Cordes, Corina Schwitzke, Hans-Jörg Bauer
Institute of Thermal Turbomachinery, Karlsruhe Institute of Technology, Karlsruhe, Germany

Abstract

Lower specific fuel consumption as well as noise reduction are the main goals in the sector of civil aeronautics engineering nowadays. One prominent concept of achieving these goals is the geared turbofan engine, in which a planetary gear box is installed between the low pressure spool and the fan. This allows the low pressure turbine as well as the fan to rotate at optimum speeds. This way, the same power can be generated by fewer stages in the faster rotating turbine, which in turn compensates the additional weight of the gear box. The main advantage of the geared turbofan is the possibility to further increase the fan diameter and therefore improve the propulsion efficiency by means of a higher bypass ratio. One crucial feature of the gear box is the cooling system needed to ensure safe operating conditions during all phases of the flight envelope. For an efficient cooling system, optimized with respect to weight and cost, the heat transfer between the cooling fluid and the gears needs to be understood thoroughly. In this study, the impingement cooling of spur gears by oil jets is for the first time examined analytically and compared to experimental results. This provides knowledge about the evolution of the heat transfer coefficient distribution resulting from the cooling fluid flow rate and the gear speed, as well as a deep understanding of the underlying phenomena causing this behavior. The analytical solution process comprises of two calculation steps. First, the size of the oil film is calculated and secondly, the heat transfer across this surface is evaluated while the oil film is flung off the tooth flank by centrifugal forces. The parameters varied in this study were the oil flow rate, the rotational speed of the spur gear and the oil jet angle. The theoretical results are in good agreement with the experimental data. The theoretical approach can therefore be applied as a new and efficient tool to estimate the global heat transfer coefficient of impingement cooled spur gears. Furthermore, the validated tool can be used as boundary condition for thermal models of spur gears and help optimize the impingement cooling oil systems.

1 INTRODUCTION

The reduction of specific fuel consumption for civil airplanes is a major goal nowadays. New regulations as well as high prices for jet fuel increase the necessity to develop more efficient jet engines. One proposal that promises to increase the overall efficiency of jet engines is the geared turbofan engine. A planetary gear box in between the low pressure turbine and the fan allows to rotate the two components at their respective ideal rotational speed. The low pressure turbine can rotate faster to decrease the number of turbine stages necessary to power the fan and the fan is slowed down to enable larger fan diameters. Such an increase in fan diameter allows for higher bypass ratios and, therefore a higher propulsion efficiency. An additional advantageous effect is the noise reduction from the deceleration of the fan.

A planetary gear box for commercial aircrafts has several challenging technical requirements. The gear box needs to transmit a high power (up to 50 MW) at high rotational speeds (up to 10,000 rpm). Furthermore, the gear box has to be small enough to be mounted inside the engine and light-weight. Finally, the gear box has to be efficient to minimize power losses and highly reliable to get approved for civil air transport.

One common failure mode of such high-speed,

doi:10.25967/490085

high-load gear boxes is scoring. The abrasive wear causing scoring starts when the lubrication is not sufficient and the meshing gears come into contact through mixed lubrication [1]. The breakdown of the lubrication film is usually associated with an increase in bulk temperature which is defined as the oil film temperature right before meshing [2]. A higher bulk temperature leads to a decrease in viscosity and a subsequently smaller lubrication film. It is, therefore, very important to exactly determine the bulk temperature to be able to prevent a scoring failure of the gears.

One way to calculate the bulk temperature before meshing is through a thermal balance of each gear [3]. These thermal models include the heat input of the meshing process as well as the heat release by oil cooling. The latter is usually realized by oil jets impinging on the rotating gears. The effects during meshing are well modeled by the Elastohydrodynamics as explained by Dowson and Higginson [2]. The heat release by impingement cooling, however, is not well understood so far.

To optimize the oil supply, a thorough understanding of the heat transfer mechanism is needed. This study aims at modeling the heat transfer of a round liquid oil jet onto a rotating spur gear. The results can then be used as a boundary condition for the thermal model of the gears as well as to optimize the oil supply system.

2 LITERATURE REVIEW

In this section, a brief literature review is presented concerning the heat transfer by impingement cooling of spur gears.

Keller et al. studied the fluid flow upon impact of the oil jet onto the gear flanks [4, 5]. They used the Smoothed Particle Hydrodynamic as well as the Volume-of-Fluid method for their numerical simulations. A good agreement to experimental images taken by Schober [6] was achieved. The numerical results present a good insight into the two-phase flow during oil jet impact and the subsequent spreading of the oil film on the gear tooth flank. However, the simulations were performed isothermally and, hence, no heat transfer coefficient could be extracted.

Akin and Townsend performed experiments with two meshing gears for different operating conditions. They took high-speed images of flow phenomena [7] and measured gear temperatures [8]. A deduction of heat transfer coefficients from the measurements is not possible however, because of the applied experimental setup. They investigated two loaded gears which combines the heat input through the meshing process as well as the oil jet cooling. Consequently, a separation between the two processes is not feasible.

DeWinter and Blok investigated the impingement cooling process analytically. Their approach modeled the physical process as a fluid film flung off the gear tooth flank by centrifugal forces [9]. Van Heijningen and Blok modified the model to include a variable viscosity of the cooling oil during the fling-off process [10]. Terauchi et al. presented a different modification to the analytical model by DeWinter and Blok to enable a finite initial coolant film height [11]. El-Bayoumy presented a simplified version of the analytical model which reduces the heat transfer to pure heat conduction [12]. Additionally, the heat transfer is limited to the thermal capacity of the oil film. The simplified model shows good agreement with the DeWinter and Blok model. Kromer et al. evaluated the heat transfer as a function of time and position on the gear tooth flank for the DeWinter and Blok model [13]. The differences in heat transfer with respect to the modified models by van Heijningen and Blok as well as Terauchi et al. were also quantified.

All of the analytical models so far calculated the heat transfer only across the gear tooth surface wetted by the oil jet. The effect of the size of the wetted surface which is dependent on the operating conditions was not included. This is the reason why the results in this study will be presented with respect to a fixed reference surface, thus enabling a comparison between different operating conditions. Furthermore, none of the analytical models have been validated against experimental data for a wide range of operating conditions. Hence, this study presents a comparison between analytical and experimental results for varying operating parameters for the first time.

3 EXPERIMENTAL INVESTIGATION

In this section the experimental setup used for the validation of the theoretical model is explained.

The experimental data stems from a previous project at the Institute of Thermal Turbomachinery (ITS) at the Karlsruhe Institute of Technology.

3.1 Experimental Setup

The test rig at ITS consists of a hollow spur gear driven by an electric motor. Furthermore, the heat transfer problem was inverted to facilitate the experiments. Instead of cooling the gear by an impinging oil jet, the jet was used to heat up the spur gear. Air impingement on the inside of the hollow spur gear was applied to cool the inside of the gear. This procedure created a temperature gradient in radial direction of the gear. The temperature was measured via thermocouples on the inside as well as the outside of the gear. The details of the geometry of the spur gear are listed in table 1.

An oil nozzle is placed above the gear to create an oil jet directed onto the rotating gear. Mobil Jet Oil II, a typical oil used in the areospace industry, was used for the experiments. The properties of the oil jet are listed in table 2.

3.2 Experimental procedure

In order to obtain the heat transfer coefficient for a specific operating condition, the following three steps were carried out. First, the test rig was started up and the operating parameters were set to the desired values. The parameters were the oil flow rate $\dot{V}$ supplied per oil jet through the oil nozzle, the rotational speed n of the spur gear and the oil jet angle β. The last one being defined as the angle between the oil jet and the circular normal at the outer radius of the gear. Hence, an oil jet with an oil jet angle of 0° is directed radially inward. The oil jet angle is defined as positive when the oil jet is pointing in the same direction as the gear rotation.

Secondly, the temperature measurements were taken when the system reached a stationary state. In a third step, a finite element model was used to solve the inverse heat transfer problem to obtain the local heat transfer coefficients across the gear tooth surface. This had to be done because no analytical solution was available for the complex geometry of the gear teeth. Since the inverse heat transfer problem cannot be solved explicitly, an iterative approach was chosen. A certain heat transfer coefficient distribution was set as boundary condition on the gear tooth surface and the temperature field inside the gear was calculated. The numerical simulations were repeated until the simulated temperatures matched the measured temperatures. The experiments resulted in a heat transfer coefficient distribution across the gear tooth surface for each operating condition. The experimental results presented in section 5 are the surface averaged values of heat transfer coefficient distributions which can be compared to the results from the theoretical model. The experimental error for the averaged heat transfer coefficient was evaluated to be below 4 %.

4 THEORETICAL MODEL

The theoretical model presented in this paper combines for the first time the analytical solution for the heat transfer in a film flung off by centrifugal forces with a model for the wetted surface. The latter is calculated by approximating the wetted surface as a rectangle on the windward gear tooth flank. The height of this rectangle is the length between the impingement point of the oil jet and the outer radius of the gear tooth flank. The width of the rectangle is calculated with an experimental correlation by Guo [14]. These two steps are described in the following subsections before the analytical solution for the heat transfer is presented. Input variables for the theoretical model in this study are the same as in the experiments, namely the oil flow rate, the rotational speed of the gear, and the oil jet angle at the outer radius. The target parameter of the theoretical model is the heat transfer coefficient averaged over the spur gear surface.

A schematic of the gear geometry is shown in figure 1. All the relevant lengths and angles are labeled according to the following theoretical model as to facilitate the description. In the schematic, two gear teeth are depicted by a thick solid line with additional dotted auxiliary lines.

4.1 Impingement depth

The impingement depth is calculated with a model by Akin und Townsend [15]. It takes into account the geometry of the gear teeth, in this

Table 1: Geometrical data of the ITS-gear

Variable	Symbol	Value	Unit
module	m	4.0	mm
number of teeth	N	65	-
pressure angle	α_p	25	°
clearance	c	1.0	mm
addendum modification coefficient	x_a	0.25	-
root fillet radius	R_f	0.8	mm
base radius	R_b	117.8	mm
root radius	R_r	126.0	mm
pitch radius	R_p	130.0	mm
outer radius	R_o	135.0	mm
tooth height	L	9.0	mm
tooth width per oil jet	W	22.5	mm

Table 2: Oil jet data

Variable	Symbol	Value	Unit
Oil jet diameter	d	1.15	mm
kinematic viscosity	ν	8.011e-6	m^2/s
Thermal conductivity	k	0.1447	W/m K
Thermal diffusivity	a	7.6e-8	m^2/s

case an involute gear, as well as the operating conditions. In the model, the rotational speed is calculated based on the impingement depth, therefore, an iterative approach is necessary. In this study, the impingement depth R_i is first set to an initial value on the gear tooth flank. The corresponding rotational speed of the gear is calculated with the help of the model and compared to the given operating conditions. In a next iteration, the impingement depth is adapted and the calculations are repeated. This is done until the relative error for the rotational speed of the gear is below 0.1 %.

The gear angle ϑ_j from the base circle to an arbitrary point j on the gear tooth flank with the gear axis at its center can be calculated by evaluating the involute function

$$\begin{aligned} \vartheta_j &= \tan\left(\alpha_j\right) - \alpha_j \\ &= \left[\left(\frac{R_j}{R_\mathrm{b}}\right)^2 - 1\right]^{\frac{1}{2}} - \arccos\left(\frac{R_\mathrm{b}}{R_j}\right) . \end{aligned} \tag{1}$$

The gear angle of any point on the gear tooth flank can then be found by replacing the index j with the desired index, e.g. the outer radius with index o. With the help of equation 1, the angle of the leeward side can be determined as

$$\vartheta_\mathrm{lee} = \vartheta_\mathrm{o} - \vartheta_\mathrm{r} . \tag{2}$$

The gear angle of the bottomland has to take into

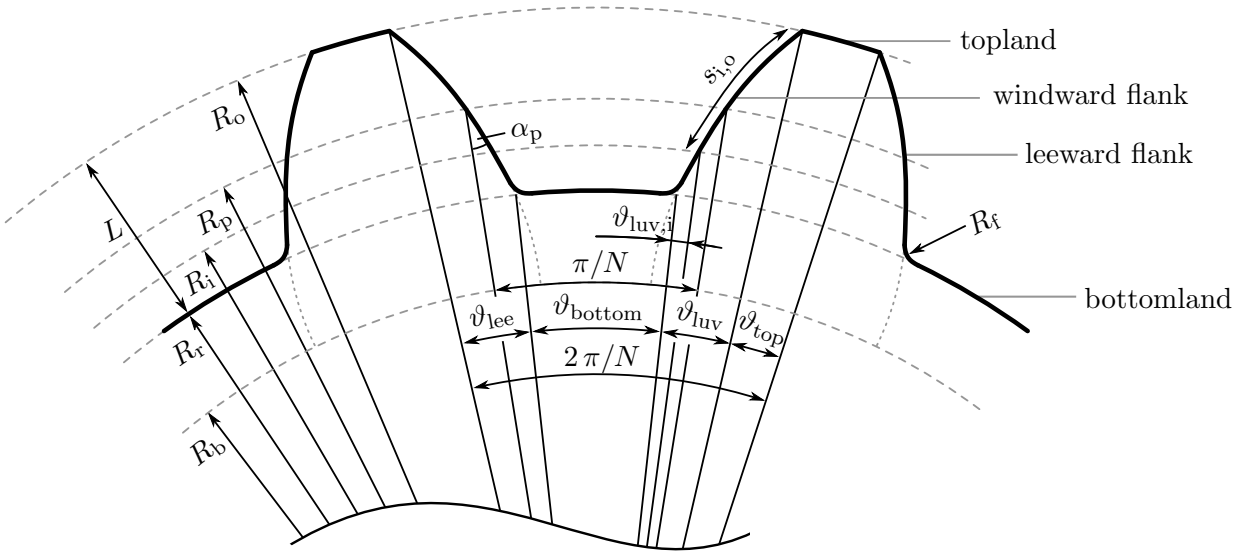

Figure 1: Schematic of the spur gear geometry

account the addendum modification to yield

$$\vartheta_{\mathrm{bottom}} = \frac{\pi}{N} - 2\,(\vartheta_{\mathrm{p}} - \vartheta_{\mathrm{r}}) - \frac{2x_{\mathrm{a}}\tan(\alpha_{\mathrm{p}})}{R_{\mathrm{p}}}\,. \tag{3}$$

On the windward side of the gear tooth, the gear angle from the root radius up to the impingement depth can be determined to

$$\vartheta_{\mathrm{luv,i}} = \vartheta_{\mathrm{i}} - \vartheta_{\mathrm{r}}\,. \tag{4}$$

An additional angle comes into play for a jet which is not directed radially inward, but at an angle β tilted from the radial direction. The angle is defined at the outer radius as

$$\vartheta_{\mathrm{jet}} = \mathrm{sign}(\beta)\arccos\left(\frac{R_{\mathrm{i}}^2 + R_{\mathrm{o}}^2 - F^2}{2\,R_{\mathrm{i}}\,R_{\mathrm{o}}}\right)\,, \tag{5}$$

with the length of the flight path of the oil jet starting from the outer radius F defined as

$$F = R_{\mathrm{o}}\cos(\beta) - \left(R_{\mathrm{o}}^2\,\cos^2(\beta) - R_{\mathrm{o}}^2\,R_{\mathrm{i}}^2\right)^{\frac{1}{2}}\,. \tag{6}$$

The sum of these four angles is the total angle rotated by the gear from the time the oil jet penetrates the gear tooth space until it impinges on the gear flank at the impingement depth. This angle

$$\vartheta_{\mathrm{tot}} = \vartheta_{\mathrm{lee}} + \vartheta_{\mathrm{bottom}} + \vartheta_{\mathrm{luv,i}} + \vartheta_{\mathrm{jet}} \tag{7}$$

can subsequently be used to calculate the rotational speed at the set impingement depth

$$n = \frac{30\,v_{\mathrm{jet}}\,\vartheta_{\mathrm{tot}}}{\pi\,F}\,, \tag{8}$$

with the jet velocity defined as

$$v_{\mathrm{jet}} = \frac{4\,\dot{V}}{\pi\,d^2}\,. \tag{9}$$

The described model represents a single iteration which has to be repeated until the desired accuracy is reached. One restriction occurs in the calculation process of the impingement depth, which is the fact that the impingement depth cannot exceed the gear tooth height. The restriction implies that the theoretical model is limited to operating conditions where the oil jet is only impinging on the windward side and not the leeward side or the bottomland.

4.2 Wetted length per unit time

With the impingement depth now determined, the wetted length on the gear surface needs to be calculated. For one gear tooth, it corresponds to the arc length on the involute spur gear between the impingement depth and the outer radius

$$s_{\mathrm{i,o}} = \frac{R_{\mathrm{o}}^2 - R_{\mathrm{i}}^2}{2\,R_{\mathrm{b}}}\,. \tag{10}$$

When the arc length is multiplied by the number of teeth and the rotational speed of the gear, the wetted length per unit time results to

$$\dot{s}_{\mathrm{i,o}} = \frac{n\,s_{\mathrm{i,o}}\,N}{60}\,. \tag{11}$$

4.3 Width of the oil film

The width of the oil film after the impingement process is approximated by using the empirical correlation by Guo [14]. In his study, the oil film width of a fluid jet impinging on a rotating plate was measured over a wide range of jet Reynolds numbers as well as jet and surface velocities. When the surface velocity is replaced by the wetted length per unit time, the oil film width can be described as

$$W_{\mathrm{l}} = 0.359\,d\,\left(\frac{v_{\mathrm{jet}}}{\dot{s}_{\mathrm{i,o}}}\right)^{\frac{1}{2}}\mathrm{Re}_{\mathrm{jet}}{}^{\frac{1}{2}} \tag{12}$$

with

$$\mathrm{Re}_{\mathrm{jet}} = \frac{v_{\mathrm{jet}}\,d}{\nu}\,. \tag{13}$$

However, several oil jets impinged at a certain distance in the experiments, hence, the width of the fluid film cannot exceed the width of the gear per oil jet W. This is why the restriction $W_{\mathrm{l}} \leq W$ is applied.

4.4 Wetted tooth flank surface

With the knowledge of the wetted length per unit time and the oil film width, it is now possible to deduct the wetted surface on each windward tooth flank. The impingement process takes place once per revolution which leads to the wetted surface per unit time

$$\dot{A}_{\mathrm{oil}} = \dot{s}_{\mathrm{i,o}}\,W_{\mathrm{l}}\,. \tag{14}$$

To be able to compare different operating conditions, it is important to relate the heat transfer to the same surface area. This is the reason why a reference surface is chosen because the wetted surface depends on the operating condition. The reference surface is defined as the surface of the spur gear excluding the side surfaces of the gear. The reference surface for one gear tooth comprises of the bottomland, the topland and the two gear flanks (windward and leeward side). Its length in circumferential direction s_{tooth} is defined as

$$s_{\mathrm{tooth}} = \frac{R_{\mathrm{o}}^2 - R_{\mathrm{r}}^2}{R_{\mathrm{b}}} + \vartheta_{\mathrm{bottom}}\,R_{\mathrm{r}} + \vartheta_{\mathrm{top}}\,R_{\mathrm{o}} + (\pi - 4)R_{\mathrm{f}}\,. \tag{15}$$

The last term in the equation takes into account the effect of the fillets at the root of each gear flank on the reference surface. The gear angle for the topland ϑ_{top} can be calculated with the help of the gear angles in section 4.1

$$\vartheta_{\mathrm{top}} = \frac{2\,\pi}{N} - 2(\vartheta_{\mathrm{o}} - \vartheta_{\mathrm{r}}) - \vartheta_{\mathrm{bottom}}\,. \tag{16}$$

The reference surface per unit time $\dot{A}$ can subsequently be determined by multiplying the reference length with the rotational speed n an the number of teeth N

$$\dot{A} = \frac{n\,s_{\mathrm{tooth}}\,N\,W}{60}\,. \tag{17}$$

4.5 Heat transfer across wetted surface

The heat transfer from the gear surface to the oil film was first analytically described by DeWinter and Blok [9]. They considered a coolant film of infinite initial film height. The film is at temperature T_0 at the start of the process while the gear tooth surface remains at a higher constant temperature T_{wall} throughout the process. While the oil film is flung off the gear tooth by centrifugal forces, it is heated by the gear tooth surface. The viscosity as well as all other material properties are assumed to be constant during the process with the values listed in table 2.

With the help of the temperature field in the oil film calculated by the analytical model, the heat transfer at the gear tooth surface can be evaluated. The temperature gradient across the surface is used to obtain the local heat transfer coefficient. By averaging over the gear tooth surface in space and over one revolution in time a global heat transfer coefficient over the wetted surface $h_{\mathrm{i,o},\infty}$ is calculated. This heat transfer coefficient was evaluated by Kromer et al. [13] to

$$h_{\mathrm{i,o},\infty} = 0.0505\, k \left(\frac{\nu\, L\, n^2}{R_\mathrm{p}\, a^3} \right)^{\frac{1}{4}} . \tag{18}$$

The sole restriction is that the following condition has to be fulfilled [13]

$$s_\mathrm{i,o} < \frac{4\,\pi^2\, R_\mathrm{p}\, a}{\psi_\mathrm{end}^4\, \nu} . \tag{19}$$

This can be interpreted as the heat transfer being finished after one revolution and, therefore, that the whole oil film has reached the wall temperature. The parameter ψ_end is approximately 1.5 [13]. The restriction is fulfilled for all the cases investigated in this study.
Kromer et al. also evaluated the modified analytical model presented by Terauchi et al. [11]. The modification allows to include the effect of a finite initial coolant film height on the heat transfer. The results for the heat transfer coefficient of the finite initial coolant film height were presented in relation to the infinite initial coolant film height. The ratio can be approximated by

$$\begin{aligned} \frac{h_\mathrm{i,o}}{h_{\mathrm{i,o},\infty}} = {} & -0.07477\psi_0^4 + 0.4262\psi_0^3 \\ & - 0.7611\psi_0^2 + 0.1208\psi_0 + 0.9907 \end{aligned} \tag{20}$$

as a function of the dimensionless time variable at the start of the process ψ_0

$$\psi_0 = \frac{3.651}{\bar{H}_0} \left(\frac{\nu\, a\, L}{\pi^2\, n^2\, R_\mathrm{p}} \right)^{\frac{1}{4}} . \tag{21}$$

The average initial coolant film height $\bar{H}_0$ needs to be known which can be derived from the oil flow rate $\dot{V}$ and the wetted surface per unit time $\dot{A}_\mathrm{oil}$

$$\bar{H}_0 = \frac{\dot{V}}{\dot{A}_\mathrm{oil}} . \tag{22}$$

Equation 20 is only valid for $\psi_0 < 2$ according to Kromer et al. [13]. This restriction is met for all the cases investigated in this study.

4.6 Global heat transfer

The global heat transfer coefficient is the heat transfer coefficient on the reference surface per unit time. Any parts of the reference surface that are not wetted by the impinging jet are assumed to be adiabatic. The global heat transfer coefficient h can be evaluated by combining the results of the previous subsections to

$$h = h_{\mathrm{i,o},\infty} \frac{h_\mathrm{i,o}}{h_{\mathrm{i,o},\infty}} \frac{\dot{A}_\mathrm{oil}}{\dot{A}} . \tag{23}$$

5 RESULTS

In the following section, the results of the theoretical model will be presented. The influence of the three parameters of the experiments, the oil flow rate, the rotational speed and the oil jet angle on the heat transfer mechanism are investigated. The theoretical data is compared to the experimental data from the experiments described in section 3. This way, the theoretical model is validated and possible differences are discussed. All data will be presented in a normalized fashion.

5.1 Rotational speed

The influence of the rotational speed on the heat transfer coefficient can be seen in figure 2. The heat transfer coefficient is plotted over the rotational speed for a normalized oil flow rate of $\dot{V}/\dot{V}_\mathrm{max} = 0.4$ and an oil jet angle $\beta = 20°$. It can be seen that the theoretical model is only able to predict the heat transfer for rotational speeds of $n/n_\mathrm{max} \geq 0.2$. This is caused by the restriction of the impingement depth. For lower rotational speeds the oil jet would impinge on the bottomland or possibly even the leeward tooth flank. Whenever this is the case, the theoretical model is no longer valid and, therefore, no result can be obtained. For rotational speeds higher than 0.2,

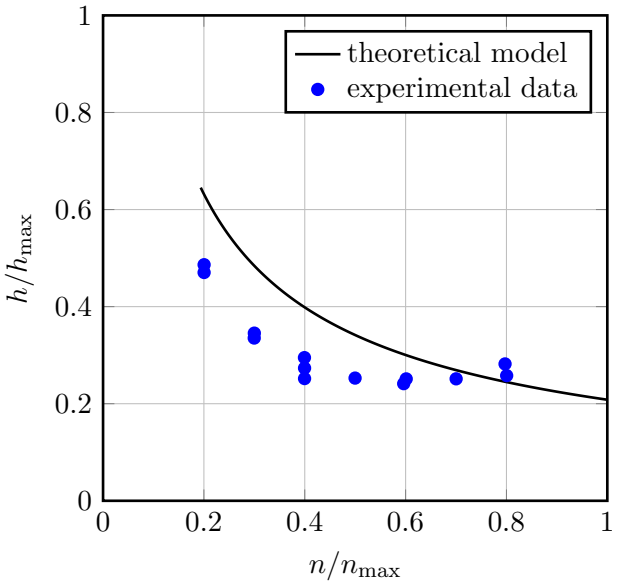

Figure 2. Theoretical results and experimental data for $\dot{V}/\dot{V}_{\max} = 0.4$ and $\beta = 20°$

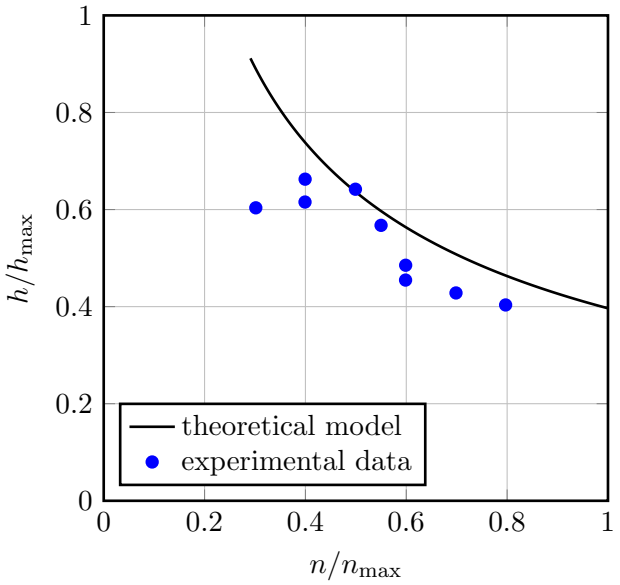

Figure 3. Theoretical results and experimental data for $\dot{V}/\dot{V}_{\max} = 0.6$ and $\beta = 20°$

the theoretical model predicts a sharp decrease in heat transfer for an increase in rotational speed. For rotational speeds higher than 0.5, the decrease is less pronounced. When the theoretical results are compared to the experimental data, a good agreement can be observed. The same general trend for the heat transfer is visible although the experimental data remains nearly constant for rotational speeds greater than 0.5. The theoretical results overestimate the heat transfer for small rotational speeds by up to 60 %.

In figure 3, the heat transfer coefficient for a higher volume flow rate of $\dot{V}/\dot{V}_{\max} = 0.6$ is shown. The theoretical results are qualitatively similar although the decrease in heat transfer is more uniform across the investigated range of rotational speeds. The theoretical model compares well with experimental data except for the lowest rotational speed of $n/n_{\max} = 0.3$ where the theoretical model predicts a heat transfer coefficient that is around 50 % higher than the experimental value. A possible reason for this behavior could be that the theoretical model over predicts the oil film width for impingement depths close to the root radius.

Overall, a decrease in heat transfer coefficient is observable for an increase in rotational speed. The main reason for this behavior is the decrease in impingement depth for increasing rotational speeds. The subsequent decrease in the wetted surface area dominates the increase in local heat transfer. This way, although the heat transfer coefficient over the wetted surface is increasing with the square root of the rotational speed, the global heat transfer coefficient is decreasing.

5.2 Oil jet angle

The influence of the oil jet angle on the heat transfer is rather small. Figures 4 and 5 depict the heat transfer coefficients for an oil jet angle of 0° for oil flow rates of $\dot{V}/\dot{V}_{\max} = 0.4$ and 0.6, respectively. The minimum rotational speed for the theoretical model is lower compared to the 20° cases. This is caused by the impingement depth which depends on the oil jet angle. The heat transfer coefficient over the wetted surface does not depend on the oil jet angle as long as the wetted surface remains the same. For both cases, the theoretical model compares well to the experimental data.

In figure 5, a qualitative difference between the theoretical and the experimental data can be observed. While the theoretical model predicts a monotonous decrease in heat transfer for increasing rotational speeds, the experimental data shows a slight increase in heat transfer for rotational speeds of $n/n_{\max} < 0.4$. This effect is not captured by the current theoretical model.

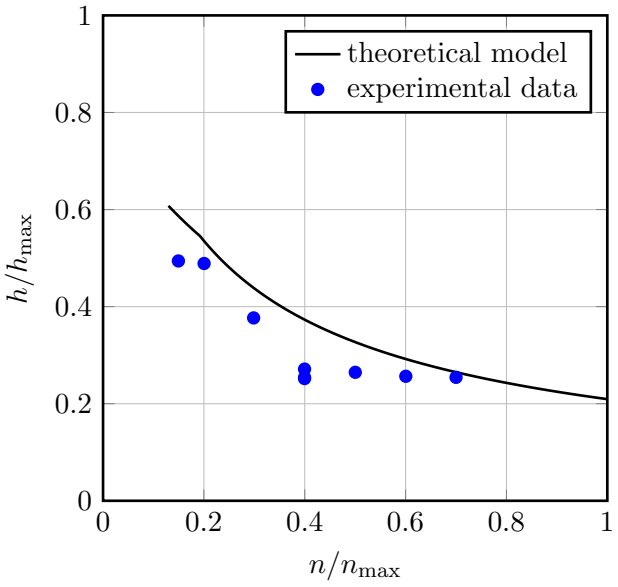

Figure 4. Theoretical results and experimental data for $\dot{V}/\dot{V}_{\max} = 0.4$ and $\beta = 0°$

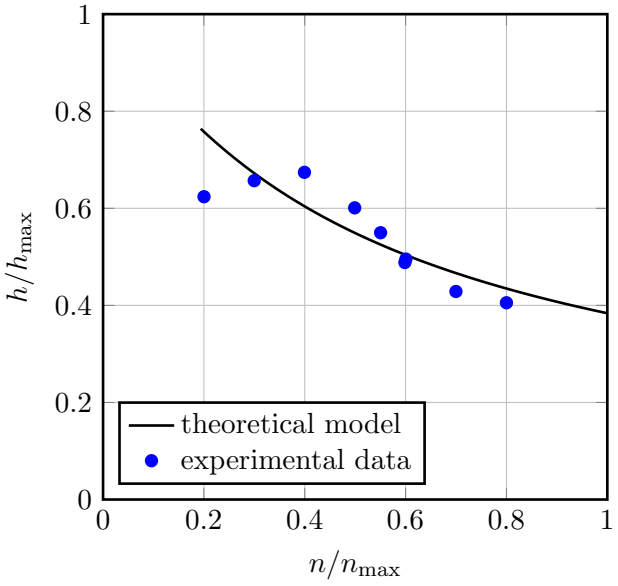

Figure 5. Theoretical results and experimental data for $\dot{V}/\dot{V}_{\max} = 0.6$ and $\beta = 0°$

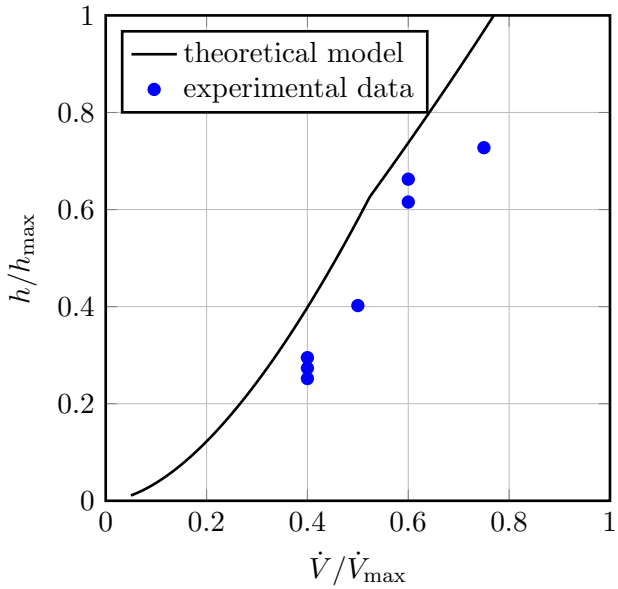

Figure 6. Theoretical results and experimental data for $n/n_{\max} = 0.4$ and $\beta = 20°$

5.3 Oil flow rate

The third and final parameter investigated is the volumetric oil flow rate. In figure 6, the heat transfer coefficient is plotted over the measured range of oil flow rates for a rotational speed of $n/n_{\max} = 0.4$. The theoretical model predicts an increases in impingement depth for an increase in oil flow rate and, therefore, a larger wetted surface per unit time. Additionally, the increased impingement depth leads to a higher heat transfer over the wetted surface through the increase in wetted length L. The third factor for the steep increase in heat transfer is the wetted width. According to equation 12 the wetted width increases with increasing oil flow rate. At $\dot{V}/\dot{V}_{\max} \approx 0.5$ however, a dent is visible in the theoretical results. This is due to the fact, that the wetted width reaches the maximum width of the gear per oil jet W and cannot grow any further.

Figure 7 depicts the heat transfer coefficient over oil flow rate for a higher rotational speed of $n/n_{\max} = 0.8$. The same general trend as for figure 6 can be seen with the sole difference that the slope becomes less steep for higher rotational speeds. This can be explained by the decrease in wetted surface per unit time as discussed in subsection 5.1. The theoretical model predicts the heat transfer well over the entire range of investigated oil flow rates and rotational speeds.

6 SUMMARY

In this study, the heat transfer of a spur gear cooled by oil jet impingement is investigated. A theoretical model is derived to determine the heat transfer coefficient in relation to a reference surface. The entire gear surface excluding the side surfaces is chosen as the reference surface. First, the surface wetted by the impinging oil jet and

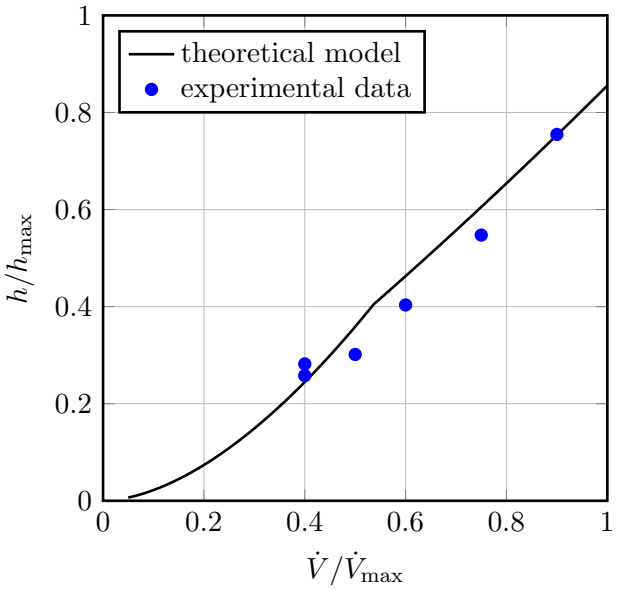

Figure 7. Theoretical results and experimental data for $n/n_{\max} = 0.8$ and $\beta = 20°$

the subsequent spreading of the oil film over the gear tooth flank is calculated. Secondly, the heat transfer between the gear and the oil film is evaluated. The resulting heat transfer coefficients show very good agreement with experimental data. A parameter study unveils the influence of the parameters oil flow rate, rotational speed and oil jet angle. Increasing the oil flow rate leads to a strong increase whereas an increase in rotational speed leads to a decrease in heat transfer. The oil jet angle has very little impact on the heat transfer mechanism. In conclusion, this study presents a new and validated approach to quantify the heat transfer of impingement cooled spur gears.

Acknowledgments

The authors would like to thank the Dr.-Ing. Willy-Höfler-Stiftung for their funding.

Nomenclature

Latin symbols

A	surface
$\dot{A}$	surface per unit time
a	thermal diffusivity of the oil
c	clearance
d	oil jet diameter
F	length of oil jet flight path
h	heat transfer coefficient
H	oil film height
$\bar{H}$	average oil film height
k	thermal conductivity of the oil
L	tooth height
m	gear module
N	number of teeth
n	rotational speed [rpm]
R	radius
Re	Reynolds number
s	arc length on gear tooth flank
$\dot{s}$	arc length per unit time
T	temperature
$\dot{V}$	oil flow rate
v	velocity
W	gear tooth width per oil jet
x_{a}	addendum modification coefficient

Greek symbols

α	pressure angle
β	oil jet angle at outer radius
ϑ	gear angle
ν	kinematic viscosity
ψ	dimensionless time variable

Indizes

b	base
bottom	bottomland
end	end of the process
f	root fillet
g	global
i	impingement point
j,k	random point on gear tooth flank
jet	oil jet flight path
l	oil film
lee	leeward side
luv	windward side
max	maximum
o	outer
oil	wetted by the oil jet
p	pitch
r	root
tooth	gear tooth
top	topland
tot	total
0	at the start of the process
∞	infinite initial film height

References

[1] Spikes, H. A., 1997. "Mixed lubrication — an overview". *Lubrication Science,* **9**(3), pp. 221–253.

[2] Dowson, D., Higginson, G. R., and Hopkins, D. W., 1977. *Elasto-Hydrodynamic Lubrication: International Series on Materials Science and Technology*, 2 ed., Vol. v.23 of *International Series on Materials Science and Technology*. Elsevier Science, Burlington.

[3] Patir, N., and Cheng, H. S., 1979. "Prediction of the Bulk Temperature in Spur Gears Based on Finite Element Temperature Analysis". *A S L E Transactions,* **22**(1), pp. 25–36.

[4] Keller, M. C., Braun, S., Wieth, L., Chaussonnet, G., Dauch, T. F., Koch, R., Schwitzke, C., and Bauer, H.-J., 2017. "Smoothed Particle Hydrodynamics Simulation of Oil-Jet Gear Interaction". In Proceedings of ASME Turbo Expo 2017, p. V02BT41A019.

[5] Keller, M. C., Braun, S., Wieth, L., Chaussonnet, G., Dauch, T. F., Koch, R., Schwitzke, C., and Bauer, H.-J., 2019. "Smoothed Particle Hydrodynamics Simulation of Oil-jet Gear Interaction". *Journal of Tribology,* **141**(7).

[6] Schober, H., 1983. "Einspritzschmierung bei Zahnradgetrieben". Dissertation, Universität Stuttgart, Stuttgart.

[7] Akin, L. S., Mross, J. J., and Townsend, D. P., 1975. "Study of lubricant jet flow phenomena in spur gears". *Journal of Lubrication Technology,* **97**(2), pp. 283–288.

[8] Townsend, D. P., and Akin, L. S., 1981. "Gear Lubrication and Cooling Experiment and Analysis". *Journal of Mechanical Design,* **103**(4), pp. 219–226.

[9] DeWinter, A., and Blok, H., 1974. "Fling-Off Cooling of Gear Teeth". *Journal of Engineering for Industry,* **96**(1), p. 60.

[10] van Heijningen, G. J., and Blok, H., 1974. "Continuous as against intermittent fling-off cooling of gear teeth". *Journal of Lubrication Technology,* **96**(4), pp. 529–538.

[11] Terauchi, Y., Nagamura, K., and Wu, C.-L., 1989. "On Heat-Balance of Gear-Meshing Apparatus: Experimental and Analytical Heat Transfer Coefficient on Tooth Faces". *JSME international journal. Ser. 3, Vibration, control engineering, engineering for industry,* **32**(3), pp. 467–474.

[12] El-Bayoumy, E., Akin, L. S., Townsend, D. P., and Choy, F. C., 1989. "The role of thermal and lubricant boundary layers in the transient thermal analysis of spur gears". In Fifth International Power Transmission and Gearing Conference.

[13] Kromer, C., Cordes, L., Keller, M. C., Schwitzke, C., and Bauer, H.-J., 2019. "Analytical Solution to the Heat Transfer in Fling-off Cooling of Spur Gears". *Journal of Heat Transfer.*

[14] Guo, Y., 2014. "Newtonian and viscoelastic liquid jet impingement on a moving surface". PhD thesis, University of British Columbia.

[15] Akin, L. S., and Townsend, D. P., 1989. "Lubricant Jet Flow Phenomena in Spur and Helical Gears with Modified Addendums - for Radially Directed Individual Jets". In Fifth International Power Transmission and Gearing Conference.